Wave Motion 15 (1992) 43-59 Elsevier

Longitudinal wave scattering from a partially bonded fiber

Yang Yang and Andrew Norris

Department of Mechanics and Materials Science, Rutgers University, Piscataway, NJ 08855-0909, USA

Received 21 February 1991, Revised 11 July 1991

Analytical and numerical results are presented for in-plane longitudinal wave pulse scattering from a partially bonded circular fiber. The debonding is assumed to be a curved interface crack with non-contacting faces. The problem is cast in terms of the unknown stresses on the neck joining the fiber and matrix, which are found by solving a truncated set of equations in the frequency domain. Computations for both the scattering cross-sections and the dynamic stress intensity factors on the crack tips show that a strong rattling resonance occurs at a very low frequency when the neck becomes sufficiently small in extent. Transient responses are obtained for pulse incidence through the use of an inverse Fourier transform on the corresponding time harmonic solutions. Based upon the numerical results, it is suggested that the presence of the low frequency resonance may provide a feasible way to experimentally determine the extent of fiber debonding.

1. Introduction

The study of elastic waves scattered by interface cracks is of practical importance to the application of nondestructive evaluation of composite materials and has therefore received considerable attention in recent years. A brief review of earlier investigations on crack scattering in homogeneous materials was given by Kraut [1]. One of the first dynamic studies of an interface crack was due to Neerhoff [2] who considered the problem of Love waves diffracted by a flat crack of finite width situated along the interface of a layered composite. Neerhoff used an integral equation method in which the diffracted field was represented by the unknown crack opening displacement (COD). The COD was subsequently expanded in terms of Chebyshev polynomials and an infinite system of linear algebraic equations was derived for the coefficients of the polynomials. Using a similar approach, Boström [3] considered SH waves scattered from a flat interface crack between two dissimilar elastic half-planes. Since this method does not involve the use of a Green function the problem is solved in a relatively simple and straightforward manner.

Coussy [4, 5] first attacked the problems of SH waves and in-plane waves scattered from an arc-shaped interface crack between a circular fiber and its surrounding homogeneous matrix. She obtained closed form solutions which are valid in the long-wavelength, or Rayleigh limit, by the use of a perturbation method [4] and a homogenization procedure [5]. The same problem was solved numerically at finite frequencies by Yang and Norris [6] for incident SH waves using the approach similar to that of Neerhoff [2], Krenk and Schmidt [7] and Boström [3]. The numerical results of Yang and Norris [6] illustrate that the fiber can exhibit a strong resonance even at very low frequencies provided that the neck joining the fiber and matrix is sufficiently small. This resonance was not predicted by the quasistatic theory [4, 5]. Furthermore, an asymptotic solution for small values of the neck was derived by Norris and Yang [8] to explain the resonant phenomenon. The analysis is analogous to that of Burrows [9] in his discussions of gravity water waves incident on a circular harbor.

It is worthwhile to mention that Kitahara, Nakagwa and Achenbach [10] have considered the scattering problem from a spherical inclusion by a different approach. In their work the interface is modeled as a distribution of springs between the inclusion and matrix, and the case of a partial debonding is included by setting the spring constants to zero over the surfaces of the crack. On the bonded interface the tractions are assumed to be continuous, but the displacements may be discontinuous. The problem is solved by the boundary element method which although it is a powerful technique, cannot go to very high frequencies in practice. The present method can be used to consider fairly high values of the excitation frequency, and also provides the dynamic stress intensity factors in a straightforward manner. Scattering by non-planar cracks has been considered by Boström and Olsson [11] using the null field approach. The same method could, in principle, be used to study three dimensional interface cracks, although no one has yet applied it to this problem.

We consider the problem of scattering of in-plane waves from a circular fiber partially bonded to an otherwise homogeneous isotropic elastic medium. The corresponding static problem has been solved by Toya [12] and his results demonstrate the unrealistic oscillatory character of the stresses in a small region around the crack tips. For simplicity, we ignore this oscillatory behavior by considering material combinations for which the oscillation parameter vanishes. We still assume that the local stress near the crack tips has the singular behavior like $d^{-1/2}$, where d is the distance from the crack tips. Two distinct approaches can be taken, depending on whether the problem is formulated in terms of the unknown COD or in terms of the unknown tractions on the bonded neck. These methods were discussed for the SH problem by Yang and Norris [6] and Norris and Yang [8], respectively. The solution here will be developed using the stress approach since the COD approach seems much more complicated algebraically for the in-plane problem. The problem is solved in the frequency domain by the superposition of the scattered field from a cavity, which is derived in Section 2, and the additional field generated by a partially jointed fiber, discussed in Section 3. In the present analysis the additional field is first represented in terms of integrals of the unknown stresses on the bonded part of the fiber/matrix interface. The unknown stresses are then expanded in terms of Chebyshev polynomials of the first type. The coefficients of the polynomials can be determined by the continuity conditions on the interface. Subsequently, displacements, the scattering cross-section, and dynamic stress intensity factors are obtained. Finally, the scattering of a longitudinal in-plane pulse is considered and the relation between the scattered signals and the debonding size is discussed.

2. General formulation for plane strain wave incidence

2.1. Definitions and preliminaries

The displacement vector for the present plane strain problem can be decomposed into two potentials ϕ and ψ

$$u = \nabla \phi - \nabla \times \psi e_z, \tag{1}$$

where (e_r, e_θ, e_z) are cylindrical coordinates. Also, $\phi(r, \theta, t)$ and $\psi(r, \theta, t)$ satisfy the wave equations

$$\nabla^2 \phi = \frac{1}{c_{\rm L}^2} \frac{\partial^2 \phi}{\partial t^2}, \qquad \nabla^2 \psi = \frac{1}{c_{\rm T}^2} \frac{\partial^2 \psi}{\partial t^2},\tag{2}$$

where the longitudinal and transverse wave speeds are

$$c_{\rm L} = \sqrt{\frac{\lambda + 2\mu}{\rho}}, \qquad c_{\rm T} = \sqrt{\frac{\mu}{\rho}}.$$
 (3)

Define the Fourier transform pair for any real causal quantity g(t) as

$$\hat{g}(\omega) = \int_0^\infty g(t) e^{i\omega t} dt, \qquad g(t) = \frac{1}{\pi} \operatorname{Re} \int_0^\infty \hat{g}(\omega) e^{-i\omega t} d\omega$$
 (4)

where the hat over a variable represents its Fourier transform. The transformed potentials satisfy the Helmholtz equations

$$\nabla^2 \hat{\boldsymbol{\phi}} + k_{\rm L}^2 \hat{\boldsymbol{\phi}} = 0, \qquad \nabla^2 \hat{\boldsymbol{\psi}} + k_{\rm T}^2 \hat{\boldsymbol{\psi}} = 0, \tag{5}$$

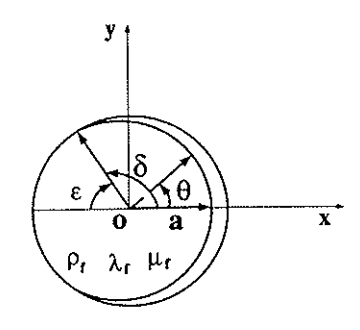
where the wavenumbers are

$$k_{\rm L} = \omega/c_{\rm L}, \qquad k_{\rm T} = \omega/c_{\rm T}.$$
 (6)

We will first obtain steady-state solutions to eqs. (5) in the frequency domain, and then perform an inverse Fourier transform defined by eq. (4), to obtain transient responses for a plane pulse.

In particular, we consider the incident plane longitudinal wave, $\hat{u}^{in} = \nabla \hat{\phi}^{in}$, propagating in the direction of the x-axis, see Fig. 1. Thus,

$$\hat{\phi}^{\text{in}} = \phi_0 \, e^{ik_L^m r \cos \theta} = \phi_0 \, \sum_{\rho=0}^{\infty} \, \varepsilon_\rho i^\rho J_\rho(k_L^m r) \, \cos p \, \theta, \qquad \hat{\psi}^{\text{in}} = 0, \tag{7}$$



ρ_{տ λտ} μտ



Fig. 1. A single circular fiber partially bonded to a homogeneous isotropic matrix.

where $\varepsilon_0 = 1$ and $\varepsilon_p = 2$, for p > 0; superscript m indicates quantities associated with the matrix, and ϕ_0 is the amplitude of the incident wave. For instance, if the incident displacement pulse is

$$u_x^{\text{in}} = U_0 u^{\text{in}} \left(t - \frac{x}{c_1^m} \right), \qquad u_y^{\text{in}} = 0,$$
 (8)

then

$$\phi_0 = \frac{U_0}{ik_1^m} \hat{u}^{\text{in}}(\omega). \tag{9}$$

2.2. Solution for a cavity

Before considering the debonded fiber, it is necessary to solve the simpler problem of scattering from a cylindrical void. We represent the total displacement as a superposition,

$$\hat{\boldsymbol{u}}^{\text{tot}} = \hat{\boldsymbol{u}}^{\text{in}} + \hat{\boldsymbol{u}}^{(0)}, \quad r > a, \tag{10}$$

where \hat{u}^{in} and $\hat{u}^{(0)}$ are the displacements of the incident field and the scattered field from the cavity, respectively. The two potentials of the scattered field are expressed as

$$\hat{\phi}^{(0)} = \phi_0 \sum_{p=0}^{\infty} A_p^{(0)} H_p^{(1)}(k_L^m r) \cos p\theta, \tag{11}$$

$$\hat{\psi}^{(0)} = \phi_0 \sum_{p=1}^{\infty} B_p^{(0)} H_p^{(1)}(k_T^m r) \sin p\theta, \tag{12}$$

which are symmetric and antisymmetric about the line $\theta = 0$, respectively. Note that $H_n^{(1)}$ is used to denote Hankel functions of the first kind and J_n are Bessel functions.

The displacement vector of the scattered field follows as

$$\hat{u}^{(0)} = \hat{u}_r^{(0)} e_r + \hat{u}_\theta^{(0)} e_\theta = \frac{\phi_0}{r} \sum_{p=0}^{\infty} T_p(\theta) A H_p^m(r) E_p^{(0)}, \tag{13}$$

where

$$T_{p}(\theta) = \begin{bmatrix} \cos p\theta & 0\\ 0 & \sin p\theta \end{bmatrix},\tag{14}$$

which has the following property

$$\int_{0}^{\pi} T_{p}(\theta) T_{q}(\theta) d\theta = \begin{cases} \frac{1}{2} \pi \delta_{pq} I, & p \neq 0, \\ \pi T_{0}, & p = q = 0, \end{cases}$$

$$(15)$$

where δ_{pq} is the Kronecker delta. Also,

$$AH_{p}^{m}(r) = \begin{bmatrix} k_{L}^{m}rH_{p}^{(1)'}(k_{L}^{m}r) & -pH_{p}^{(1)}(k_{T}^{m}r) \\ -pH_{p}^{(1)}(k_{L}^{m}r) & k_{T}^{m}rH_{p}^{(1)'}(k_{T}^{m}r) \end{bmatrix}, \qquad E_{p}^{(0)} = \begin{pmatrix} A_{p}^{(0)} \\ B_{p}^{(0)} \end{pmatrix},$$
(16)

and $B_0^{(0)} = 0$. The vector form $\hat{u}^{\text{in}} = (\hat{u}_r^{\text{in}}, \hat{u}_\theta^{\text{in}})^T$ for the incident field may be expressed as

$$\hat{\boldsymbol{u}}^{\text{in}} = \frac{\phi_0}{r} \sum_{\rho=0}^{\infty} T_{\rho}(\theta) E_{\rho}^{\text{in}}, \tag{17}$$

where

$$E_p^{\text{in}} = \varepsilon_p i^p \binom{k_L^m r J_p'(k_L^m r)}{-p J_p(k_L^m r)}. \tag{18}$$

It can then be shown that the incident traction vector $\hat{\sigma}^{in} = (\hat{\sigma}_{rr}^{in}, \hat{\sigma}_{r\theta}^{in})^T$ may be written as

$$\hat{\boldsymbol{\sigma}}^{\text{in}} = \frac{2\mu_m \phi_0}{r^2} \sum_{p=0}^{\infty} \boldsymbol{T}_p(\theta) \boldsymbol{b}_p^m, \tag{19}$$

where

$$\boldsymbol{b}_{p}^{m} = \varepsilon_{p} i^{p} \begin{pmatrix} b_{1p}^{m}(r) \\ b_{2p}^{m}(r) \end{pmatrix}, \qquad b_{1p}^{m}(r) = (p^{2} - k_{T}^{m2} r^{2} / 2) J_{p}(k_{L}^{m} r) - k_{L}^{m} r J_{p}'(k_{L}^{m} r), \\ b_{2p}^{m}(r) = p J_{p}(k_{L}^{m} r) - p k_{L}^{m} r J_{p}'(k_{L}^{m} r).$$

$$(20)$$

The scattered traction vector $\hat{\boldsymbol{\sigma}}^{(0)} = (\hat{\sigma}_{rr}^{(0)}, \hat{\sigma}_{r\theta}^{(0)})^{\mathrm{T}}$ is

$$\hat{\boldsymbol{\sigma}}^{(0)} = \frac{2\mu_m \phi_0}{r^2} \sum_{p=0}^{\infty} \boldsymbol{T}_p(\theta) \boldsymbol{D} \boldsymbol{H}_p^m(r) \boldsymbol{E}_p^{(0)}, \tag{21}$$

where

$$DH_{p}^{m}(r) = \begin{bmatrix} DH_{11}^{p}(r) & DH_{12}^{p}(r) \\ DH_{21}^{p}(r) & DH_{22}^{p}(r) \end{bmatrix}, \tag{22}$$

$$DH_{11}^{p}(r) = (p^2 - k_{\mathrm{T}}^{m2} r^2 / 2) H_p^{(1)}(k_{\mathrm{L}}^{m} r) - k_{\mathrm{L}}^{m} r H_p^{(1)}(k_{\mathrm{L}}^{m} r),$$

$$DH_{21}^{p}(r) = pH_{p}^{(1)}(k_{L}^{m}r) - pk_{L}^{m}rH_{p}^{(1)'}(k_{L}^{m}r),$$

$$DH_{12}^{p}(r) = pH_{p}^{(1)}(k_{T}^{m}r) - pk_{T}^{m}rH_{p}^{(1)'}(k_{T}^{m}r),$$
(23)

$$DH_{22}^{p}(r) = (p^{2} - k_{T}^{m2}r^{2}/2)H_{p}^{(1)}(k_{T}^{m}r) - k_{T}^{m}rH_{p}^{(1)'}(k_{T}^{m}r).$$

Use of the traction free condition at the surface of the cavity r=a and the orthogonality condition (15) yields

$$E_p^{(0)} = -[DH_p^m(a)]^{-1}b_p^m(a). \tag{24}$$

This result, combined with (10), (13), (14), (16), (20), and (22), yields the exact solution to the scattered field from a void.

3. The steady-state solution for a partially debonded fiber

3.1. Preliminary definitions

The total displacement vector is now represented as

$$\hat{\boldsymbol{u}}^{\text{tot}} = \begin{cases} \hat{\boldsymbol{u}}^{\text{in}} + \hat{\boldsymbol{u}}^{(0)} + \hat{\boldsymbol{u}}_{m}^{(1)}, & r > a, \\ \hat{\boldsymbol{u}}_{f}^{(1)}, & r < a. \end{cases}$$
 (25)

The superscript 1 denotes the additional fields generated by the partially bonded fiber, and the subscripts m and f denote the fields in the matrix and fiber, respectively. Similarly, the associated total potentials are

$$\hat{\phi}^{\text{tot}} = \begin{cases} \hat{\phi}^{\text{in}} + \hat{\phi}^{(0)} + \hat{\phi}_m^{(1)}, & r > a, \\ \hat{\phi}_r^{(1)}, & r < a, \end{cases}$$

$$(26)$$

$$\hat{\psi}^{\text{tot}} = \begin{cases} \hat{\psi}^{(0)} + \hat{\psi}_{m}^{(1)}, & r > a, \\ \hat{\psi}_{f}^{(1)}, & r < a, \end{cases}$$
 (27)

and they each satisfy Helmholtz equations in their respective domains,

$$\nabla^2 \hat{\phi}_{\alpha}^{(1)} + k_1^{\alpha 2} \hat{\phi}_{\alpha}^{(1)} = 0, \qquad \nabla^2 \hat{\psi}_{\alpha}^{(1)} + k_T^{\alpha 2} \hat{\psi}_{\alpha}^{(1)} = 0, \quad \alpha = m \text{ or } f,$$
 (28)

where

$$k_{\rm L}^{\alpha} = \omega/c_{\rm L}^{\alpha}, \qquad k_{\rm T}^{\alpha} = \omega/c_{\rm T}^{\alpha}, \quad \alpha = m \text{ or } f.$$
 (29)

The solutions satisfying the radiation condition in the matrix and which are bounded at r=0 can be expanded as

$$\hat{\phi}_{m}^{(1)} = \phi_{0} \sum_{p=0}^{\infty} A_{mp}^{(1)} H_{p}^{(1)}(k_{L}^{m}r) \cos p\theta, \qquad \hat{\psi}_{m}^{(1)} = \phi_{0} \sum_{p=1}^{\infty} B_{mp}^{(1)} H_{p}^{(1)}(k_{T}^{m}r) \sin p\theta, \tag{30}$$

$$\hat{\phi}_{f}^{(1)} = \phi_0 \sum_{p=0}^{\infty} A_{fp}^{(1)} J_p(k_{\perp}^f r) \cos p\theta, \qquad \hat{\psi}_{f}^{(1)} = \phi_0 \sum_{p=1}^{\infty} B_{fp}^{(1)} J_p(k_{\perp}^f r) \sin p\theta.$$
 (31)

Denote

$$E_p^{(1)} = \begin{pmatrix} A_{mp}^{(1)} \\ B_{mp}^{(1)} \end{pmatrix}, \qquad F_p^{(1)} = \begin{pmatrix} A_{fp}^{(1)} \\ B_{fp}^{(1)} \end{pmatrix},$$
 (32)

then the additional displacement vectors in the matrix and the fiber become

$$\hat{u}_{m}^{(1)} = \hat{u}_{rm}^{(1)} e_{r} + \hat{u}_{\theta m}^{(1)} e_{\theta} = \frac{\phi_{0}}{r} \sum_{p=0}^{\infty} T_{p}(\theta) A H_{p}^{m}(r) E_{p}^{(1)},$$
(33)

$$\hat{u}_{f}^{(1)} = \hat{u}_{rf}^{(1)} e_{r} + \hat{u}_{\theta f}^{(1)} e_{\theta} = \frac{\phi_{0}}{r} \sum_{p=0}^{\infty} T_{p}(\theta) A J_{p}^{f}(r) F_{p}^{(1)}, \tag{34}$$

where $AJ_p^f(r)$ has the same expression as $AH_p^m(r)$ after replacing Hankel functions of the first kind $H_p^{(1)}$ in (16) by Bessel functions J_p , and replacing m by f. The additional traction vectors in the matrix and the fiber are expressed as

$$\hat{\sigma}_{m}^{(1)} = \frac{2\mu_{m}\phi_{0}}{r^{2}} \sum_{p=0}^{\infty} T_{p}(\theta) DH_{p}^{m}(r) E_{p}^{(1)}, \tag{35}$$

$$\hat{\sigma}_f^{(1)} = \frac{2\mu_f \phi_0}{r^2} \sum_{p=0}^{\infty} T_p(\theta) D J_p^f(r) F_p^{(1)}, \tag{36}$$

where $DJ_p^f(r)$ has the same expression as $DH_p^m(r)$ after replacing Hankel functions of the first kind in (23) by Bessel functions, and replacing m by f.

3.2. Application of the interface conditions

The total traction must be continuous over the entire interface, bonded or debonded, implying

$$\hat{\boldsymbol{\sigma}}_{m}^{(1)} = \hat{\boldsymbol{\sigma}}_{r}^{(1)}, \quad r = a, \quad 0 < \theta < \pi, \tag{37}$$

which yields

$$F_p^{(1)} = \frac{\mu_m}{\mu_f} [DJ_p^f(a)]^{-1} DH_p^m(a) E_p^{(1)}. \tag{38}$$

The interface traction is of the form

$$\hat{\sigma}_m^{(1)}(a,\,\theta) = \begin{cases} 0, & -\delta < \theta < \delta, \\ \hat{\tau}(\theta), & \delta < |\theta| < \pi, \end{cases} \tag{39}$$

where $\hat{\tau}(\theta) = \hat{\sigma}_{rr}(\theta)e_r + \hat{\sigma}_{r\theta}(\theta)e_{\theta}$ is the unknown total traction on the neck. Use of (35), (39) and (15), yields

$$E_{\rho}^{(1)} = \frac{\varepsilon_{\rho} a^2}{2\pi \phi_0 \mu_m} [DH_{\rho}^m(a)]^{-1} \int_{\delta}^{\pi} T_{\rho}(\theta) \hat{\tau}(\theta) d\theta. \tag{40}$$

The displacement continuity condition on the neck is

$$\hat{\mathbf{u}}^{\text{in}} + \hat{\mathbf{u}}^{(0)} + \hat{\mathbf{u}}_{\text{m}}^{(1)} = \hat{\mathbf{u}}_{\text{r}}^{(1)}, \quad r = a, \quad \delta < |\theta| < \pi. \tag{41}$$

Substituting from eqs. (13), (17), (33) and (34) into (41) and using eq. (38) and (40), we obtain a system of integral equations for the unknown traction,

$$\frac{a^2}{2\pi\phi_0\mu_m}\sum_{p=0}^{\infty}\varepsilon_p T_p \Lambda_p \int_{\delta}^{\pi} T_p(\theta')\hat{\tau}(\theta') d\theta' = \sum_{p=0}^{\infty} T_p(\theta) [E_p^{\text{in}} + AH_p^m(a)E_p^{(0)}], \quad \delta < |\theta| < \pi, \tag{42}$$

where

$$A_{p} = \frac{\mu_{m}}{\mu_{f}} A J_{p}^{f}(a) [D J_{p}^{f}(a)]^{-1} - A H_{p}^{m}(a) [D H_{p}^{m}(a)]^{-1}.$$
(43)

We note that the matrices A_p are symmetric, for $p = 0, 1, 2, \ldots$

3.3. Solution of the integral equations

In order to solve the integral equations (43), we expand the unknown traction on the neck in terms of Chebyshev functions of the first type,

$$\hat{\tau}(\theta) = \frac{\phi_0 \mu_m k_L^{m^2}}{\sqrt{1 - ((\pi - \theta)/\varepsilon)^2}} \sum_{n=0}^{\infty} \boldsymbol{\Phi}_n(\theta) \boldsymbol{\beta}_n, \tag{44}$$

where $\beta_n = \beta_{1n}e_r + \beta_{2n}e_\theta$, $\varepsilon = \pi - \delta$, and

$$\boldsymbol{\Phi}_0(\theta) = \begin{bmatrix} 1 & 0 \\ 0 & 0 \end{bmatrix}, \qquad \boldsymbol{\Phi}_n(\theta) = (-1)^n \begin{bmatrix} T_{2n}((\pi - \theta)/\varepsilon) & 0 \\ 0 & T_{2n-1}((\pi - \theta)/\varepsilon) \end{bmatrix}, \quad n > 0, \tag{45}$$

$$T_m \left(\frac{\pi - \theta}{\varepsilon} \right) = \cos \left(m \arccos \left(\frac{\pi - \theta}{\varepsilon} \right) \right), \quad m = 1, 2, \dots$$
 (46)

We note that this choice of basis functions permits the traction to have the usual inverse square root singularity characteristic of cracks in bulk material, but does not include the possibility of oscillatory singularities that are predicted for interface cracks. This aspect is discussed further in Section 5.

The matrices of (45) have the following useful property

$$\int_{\delta}^{\pi} \frac{T_{p}(\theta) \Phi_{n}(\theta)}{\sqrt{1 - ((\pi - \theta)/\varepsilon)^{2}}} d\theta = (-1)^{p} \frac{\pi \varepsilon}{2} J_{n}(p \varepsilon), \tag{47}$$

where

$$J_0(p\varepsilon) = \begin{bmatrix} J_0(p\varepsilon) & 0 \\ 0 & 0 \end{bmatrix}, \qquad J_n(p\varepsilon) = \begin{bmatrix} J_{2n}(p\varepsilon) & 0 \\ 0 & J_{2n-1}(p\varepsilon) \end{bmatrix}, \quad n > 0.$$
 (48)

Therefore, multiplying $\Phi_m(\theta)$ on both sides of the integral equations (43) and integrating θ over $[\delta, \pi]$, finally yields a system of linear equations for the unknown traction vector coefficients β_p ,

$$\sum_{n=0}^{\infty} \frac{\Lambda_{00}}{2} \delta_{m0} \delta_{n0} \boldsymbol{\beta}_n + \sum_{n=1}^{\infty} \left(\sum_{p=1}^{\infty} \boldsymbol{J}_m(p\varepsilon) \boldsymbol{\Lambda}_p \boldsymbol{J}_n(p\varepsilon) \right) \boldsymbol{\beta}_n = \frac{2}{\varepsilon} (k_{\perp}^m a)^{-2} \sum_{p=0}^{\infty} (-1)^p \boldsymbol{J}_m(p\varepsilon) (\boldsymbol{E}_p^{\text{in}} + \boldsymbol{A} \boldsymbol{H}_p^m(a) \boldsymbol{E}_p^{(0)}), \tag{49}$$

where

$$\Lambda_{00} = \frac{\mu_m}{\mu_f} A J_{11}^0(a) [D J_{11}^0(a)]^{-1} - A H_{11}^0(a) [D H_{11}^0(a)]^{-1}. \tag{50}$$

The eqs. (49) can also be written as

$$\sum_{n=0}^{\infty} Q_{mn} \beta_n = N_m, \quad m = 0, 1, 2, \dots,$$
 (51)

where

$$N_m = \frac{2}{\varepsilon} \sum_{p=0}^{\infty} (-1)^p J_m(p\varepsilon) (E_p^{\text{in}} + AH_p(a)E_p^{(0)}), \tag{52}$$

$$Q_{ij} = (k_{\rm L}^m a)^2 \left[\frac{\Lambda_{00}}{2} \delta_{i0} \delta_{j0} T_0 + \sum_{p=1}^{\infty} J_i(p \varepsilon) \Lambda_p J_j(p \varepsilon) \right], \quad i, j = 0, 1, 2, \dots$$
 (53)

The symmetry of Λ_p defined by (43) implies the following symmetry property

$$Q_{ii} = Q_{ii}. \tag{54}$$

This symmetry helps to simplify the numerical solution of the truncated version of the infinite set of linear equations (51).

4. The scattered fields

4.1. Far-field approximations

Using the asymptotic expansions of Hankel functions in the far-field $k_L^m r \gg 1$, we may derive the following asymptotic expressions for the scattered displacements

$$\hat{\boldsymbol{u}}_{m}^{(\zeta)} = \phi_{0} i k_{L}^{m} \left(\frac{8\pi}{k_{T}^{m} r} \right)^{1/2} e^{i(k_{L}^{m} r - \pi/4)} F_{r}^{(\zeta)}(\theta) \boldsymbol{e}_{r} + \phi_{0} i k_{T}^{m} \left(\frac{8\pi}{k_{T}^{m} r} \right)^{1/2} e^{i(k_{T}^{m} r - \pi/4)} F_{\theta}^{(\zeta)}(\theta) \boldsymbol{e}_{\theta}, \tag{55}$$

where $\zeta = 0$ denotes the scattered field of the void, $\zeta = 1$ the additional field generated by the partially bonded fiber, and the radiation patterns are

$$F_r^{(\zeta)}(\theta) = \frac{1}{2\pi} \sum_{p=0}^{\infty} (-i)^p A_{mp}^{(\zeta)} \cos p\theta,$$
 (56)

$$F_{\theta}^{(\zeta)}(\theta) = \frac{1}{2\pi} \sum_{p=1}^{\infty} (-i)^p B_{mp}^{(\zeta)} \sin p\theta.$$
 (57)

The total radiation patterns may be expressed as

$$F_r(\theta) = F_r^{(0)}(\theta) + F_r^{(1)}(\theta),$$
 (58)

$$F_{\theta}(\theta) = F_{\theta}^{(0)}(\theta) + F_{\theta}^{(1)}(\theta). \tag{59}$$

4.2. Energy conservation and the scattering cross-section

The time average of energy flux over any surface enclosing the cylinder must be zero, implying for r > a that

$$\langle P \rangle = \frac{\omega}{2} \operatorname{Im} \int_{0}^{2\pi} (\hat{\boldsymbol{u}}^{\text{in}} + \hat{\boldsymbol{u}}^{(0)} + \hat{\boldsymbol{u}}_{m}^{(1)})^{*} \cdot (\hat{\boldsymbol{\sigma}}^{\text{in}} + \hat{\boldsymbol{\sigma}}^{(0)} + \hat{\boldsymbol{\sigma}}_{m}^{(1)}) r \, d\theta = 0, \tag{60}$$

where the superscript * denotes the conjugate of a complex variable, and · denotes the inner product of two vectors. Define the total scattered energy flux as

$$\langle P^{\text{sc}} \rangle = \frac{\omega}{2} \operatorname{Im} \int_{0}^{2\pi} (\hat{\boldsymbol{u}}^{(0)} + \hat{\boldsymbol{u}}_{m}^{(1)})^{*} \cdot (\hat{\boldsymbol{\sigma}}^{(0)} + \hat{\boldsymbol{\sigma}}_{m}^{(1)}) r \, d\theta.$$
 (61)

By the use of the far-field expressions in Section 4.1, we obtain

$$\langle P^{\text{sc}} \rangle = (\lambda_m + 2\mu_m)\omega k_{\text{L}}^{m^2} |\phi_0|^2 \left\{ \sum_{p=0}^{\infty} \frac{2}{\varepsilon_p} |A_{mp}^{(0)} + A_{mp}^{(1)}|^2 + \sum_{p=1}^{\infty} |B_{mp}^{(0)} + B_{mp}^{(1)}|^2 \right\}. \tag{62}$$

The total scattering cross-section is defined as

$$\sigma(\omega) = \frac{\langle P^{\text{sc}} \rangle}{P^{\text{in}}} = \frac{2}{k_{\text{L}}^{m}} \left\{ \sum_{p=0}^{\infty} \frac{2}{\varepsilon_{p}} |A_{mp}^{(0)} + A_{mp}^{(1)}|^{2} + \sum_{p=1}^{\infty} |B_{mp}^{(0)} + B_{mp}^{(1)}|^{2} \right\}, \tag{63}$$

where the time average of the incident flux may be written as

$$P^{\text{in}} = \frac{\omega}{2} \operatorname{Im}[\hat{\mathbf{u}}^{\text{in}}(0)^* \cdot \hat{\boldsymbol{\sigma}}^{\text{in}}(0)] = \frac{\omega}{2} k_{\text{L}}^{m3} (\lambda_m + 2\mu_m) |\phi_0|^2.$$
 (64)

Letting $r \to \infty$ in (60) and using the method of stationary phase to evaluate the integrals, we deduce a relation between the total cross-section and the forward scattering amplitude

$$\sigma(\omega) = -\frac{8\pi}{k_{\rm L}^{"}} \operatorname{Re}(F_r^{(0)}(0) + F_r^{(1)}(0)). \tag{65}$$

This is the elasto-dynamic optical theorem, and will be used as a check on our numerical computations.

5. The stress intensity factors

5.1. The static stress intensity factors

Before considering numerical results, it is useful to look at the known exact results for the equivalent static problem. These should follow from the dynamic results in the limit $\omega \to 0$, and serve not only as a check on the numerical accuracy of the dynamic results but also as a reference with which to compare them. In the static case of arbitrary biaxial tensions applied at infinity, the stresses on the bonded interface are given in eq. (3.37) of Toya [12] as

$$\sigma_{rr} + i\sigma_{r\theta} = [f(\theta) + ig(\theta)]\chi^{+}(\theta), \tag{66}$$

where

$$\chi^{+}(\theta) = \frac{1}{\xi} \left(e^{i\theta} - e^{i\delta} \right)^{-1/2} \left(e^{i\theta} - e^{-i\delta} \right)^{-1/2} \left[\frac{e^{i\theta} - e^{i\delta}}{e^{i\theta} - e^{-i\delta}} \right]^{-(i/2)\log\xi}, \tag{67}$$

$$\xi = \frac{\mu_f + (3 - 4\nu_f)\mu_m}{\mu_m + (3 - 4\nu_m)\mu_f},\tag{68}$$

and v_m , v_f are the Poisson's ratios of the matrix and the fiber respectively.

We will only consider the case of $\xi=1$, ignoring oscillatory behavior near the crack tips. When $\xi\neq 1$, the unknown traction on the jointed neck can be represented by the use of Jacobi functions rather than Chebyshev functions. This introduces a great deal of extra complexity and will not be considered here. The functions $f(\theta)$ and $g(\theta)$ are given in the Appendix for $\xi=1$ in terms of the loading parameters T_{∞} and N_{∞} which denote the biaxial tensions at infinity and inclined by an angle θ_0 with respect to the direction $\theta=0^{\circ}$.

The stresses on the bonded interface can be derived from eq. (66) as

$$\sigma_{rr} = \frac{-1}{\sqrt{2(\cos\delta - \cos\theta)}} \left[f(\theta) \sin\frac{\theta}{2} - g(\theta) \cos\frac{\theta}{2} \right]$$
 (69)

$$\sigma_{r\theta} = \frac{-1}{\sqrt{2(\cos\delta - \cos\theta)}} \left[f(\theta) \cos\frac{\theta}{2} + g(\theta) \sin\frac{\theta}{2} \right]. \tag{70}$$

These results allow us to obtain explicit formulae for the static stress intensity factors, defined as

$$KI_{\rm sl} = \lim_{\theta \to \delta^+} [2a(\theta - \delta)]^{1/2} \sigma_{rr}(\theta) = -\sqrt{\frac{a}{\sin \delta}} \left[f(\delta) \sin \frac{\delta}{2} - g(\delta) \cos \frac{\delta}{2} \right],\tag{71}$$

$$KI_{s2} = \lim_{\theta \to \delta^{+}} [2a(\theta - \delta)]^{1/2} \sigma_{r\theta}(\theta) = -\sqrt{\frac{a}{\sin \delta}} \left[f(\delta) \cos \frac{\delta}{2} + g(\delta) \sin \frac{\delta}{2} \right], \tag{72}$$

where the subscripts s1 and s2 denote the first and the second (mode I and mode II, respectively) static stress intensity factors (SIF). Furthermore, the dimensionless stress intensity factors may be written in vector form

$$\frac{KI_s}{T_{co}\sqrt{a}} = \frac{1}{T_{co}\sqrt{a}} (KI_{s1}e_r + KI_{s2}e_\theta), \tag{73}$$

where, in the static limit of a longitudinal wave incident from infinity in the direction $\theta = 0^{\circ}$, we have $T_{\infty} = -\mu_m k_{\rm T}^{m^2} A$ and $N_{\infty} = (1 - 2c_{\rm T}^{m^2}/c_{\rm L}^{m^2})T_{\infty}$ and $\theta_0 = 0^{\circ}$.

5.2. The dynamic stress intensity factors

The dynamic stress intensity factor at the crack tip $\theta = \delta$ is defined by

$$KI_{d} = \lim_{\theta \to \delta^{+}} [2a(\theta - \delta)]^{1/2} \hat{\tau}(\theta), \tag{74}$$

and so it follows from (44) and (45) that

$$\frac{KI_{d}}{T_{\infty}\sqrt{a}} = -\sqrt{\varepsilon} \left(\frac{c_{\mathrm{T}}^{m}}{c_{\mathrm{L}}^{m}}\right)^{2} \sum_{n=0}^{\infty} (-1)^{n} \beta_{n},\tag{75}$$

where T_{∞} is defined in the previous subsection and the subscript d denotes dynamic results.

6. Numerical results and discussion

The dimensionless dynamic stress intensity factors at the tip of an arc shaped crack embedded in a homogeneous medium have been computed in the long-wavelength or low frequency limit and compared

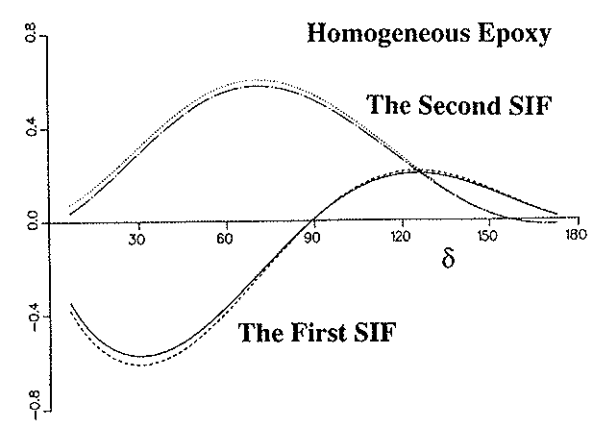


Fig. 2. The comparison of the dynamic SIFs (dash) with the static SIFs (solid) in the static limit for a crack embedded in homogeneous epoxy.

with Toya's static solutions [12]. They are displayed in Fig. 2 for an incident longitudinal plane wave. The comparison shows good agreement between eq. (75) of the present study and eq. (73) derived from Toya's theory [12]. The deviation between them could be reduced by including more terms in the expansions of the unknown stresses on the bonded interface.

Since we are more interested in problems concerning interface cracks, the remainder of the numerical computations are for the material combination of matrix and fiber given by Table 1, where the elastic shear modulus, μ_f , of the fiber has been adjusted such that the oscillatory character of stresses near the crack tips will not appear.

The magnitude of the ratios of the first dynamic stress intensity factor (DSIF) to the first static stress intensity factor (SSIF) and the second DSIF to the second SSIF are plotted in Figs. 3(a) and 4(a) for a large crack, $\delta = 170^{\circ}$. As expected, a strong resonance appears at quite a low frequency with a significant increase in the magnitude of the DSIF at the resonance frequency. The low frequency resonance is generated by the rattling of the fiber and its mechanism is similar to that encounted in the problem of SH shear wave incidence [6]. Unlike the phenomena in the case of SH-wave incidence, there are far more details in the finite and high frequency behavior of Fig. 3. These resonances at higher frequencies are due to the existence of surface waves which propagate back and forth across the faces of the crack. Figure 4(a) shows that the resonances caused by interface waves have considerably more effect on the second DSIF than the first DSIF, since surface waves are primarily shear waves and probably have a bigger contribution to shear

Table 1 The material constants for the fiber and matrix. Note that the Young's modulus of the "glass" has been adjusted so that the parameter ξ is identically unity. The modulus of glass is actually a good deal larger

Epoxy (matrix)		"Glass" (fiber)	
E_m (GN m ⁻²)	3.09	E_f (GN m ⁻²)	3.35
μ_m (GN m ⁻²)	1.28	μ_f (GN m ⁻²)	1.43
V_m	0.205	V_f	0.17
ρ _m (gm/cc)	1.25	ρ_f (gm/cc)	2.55
c_{1}^{m}/c_{T}^{m}	1.64	$ ho_f$ (gm/cc) c_L^f/c_T^f	1.59
$c_{\rm L}^m/c_{\rm L}^f$	1.40		

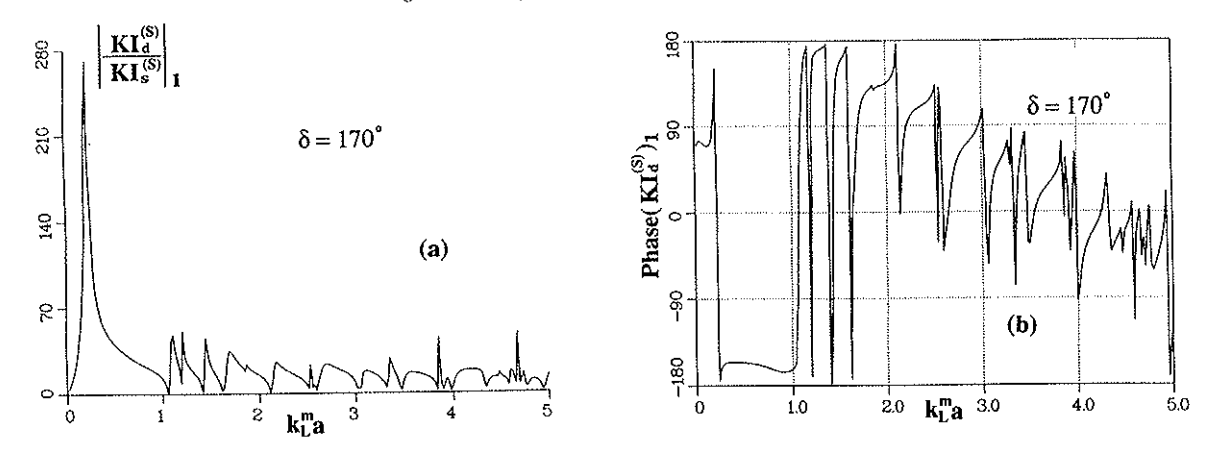


Fig. 3. (a) The magnitude of the ratio of the first dynamic SIF to the first static SIF versus nondimensional frequency $k_L^m a$, (b) the phase of the first dynamic SIF with respect to $k_L^m a$, $\theta_0 = 0^\circ$ for both (a) and (b).

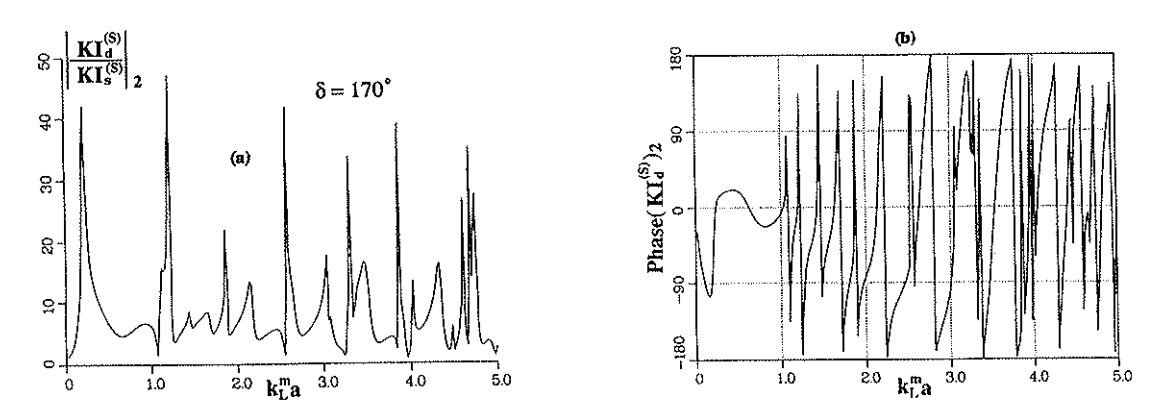


Fig. 4. (a) The magnitude of the ratio of the second dynamic SIF to the second static SIF versus nondimensional frequency $k_L^m a$, (b) the phase of the second dynamic SIF with respect to $k_L^m a$, $\theta_0 = 0^\circ$ for both (a) and (b).

stress near the crack tips. The phases of the first and second DSIFs changing with frequency are presented in Figs. 3(b) and 4(b), which clearly illustrate the characteristics of resonances.

Scattering cross-sections for different crack sizes are shown in Fig. 5, where the optical theorem has been used to check the accuracy of the numerical results. It is found that a numerical accuracy of 0.1% can be achieved when ten truncated terms are used in eq. (51) and three hundred terms are taken in the p sum in eq. (53). In Fig. 5(a), as the width of the crack is increased from zero to sixty degrees, the shapes of the curves gradually change and the low frequency resonance becomes prominent. Intuitively, one would expect that the scattering cross-section would approach that of a void when the fiber becomes almost separated from the matrix. However, this is certainly not true in the low frequency range due to the presence of the Helmholtz resonance, see Fig. 5(b).

Figure 6 shows the radial or longitudinal and the angular or shear parts of the radiation patterns at four different values of frequency for a plane harmonic wave incident on a partially bonded fiber with $\delta = 170^{\circ}$, see Figs. 6(a) and (b), and a void, see Figs. 6(c) and (d), in the direction of $\theta_0 = 0^{\circ}$. Comparing Fig. 6(a) with (c) and (b) with (d), we note that the radiation patterns generated by the partially bonded fiber and

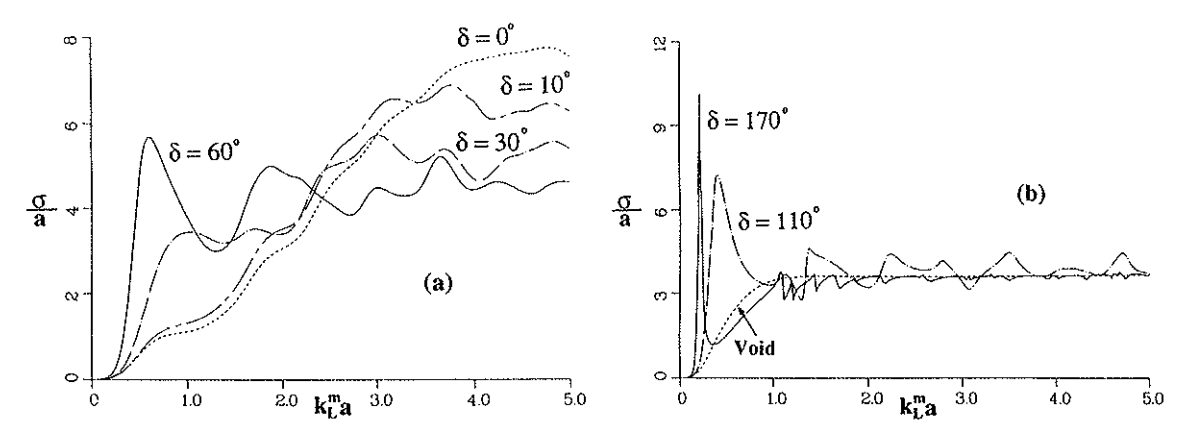


Fig. 5. The scattering cross-section for glass/epoxy, $\theta_0 = 0^\circ$, $\delta = 0^\circ$, 10° , 30° and 60° in (a) and $\delta = 110^\circ$, 170° and void in (b).

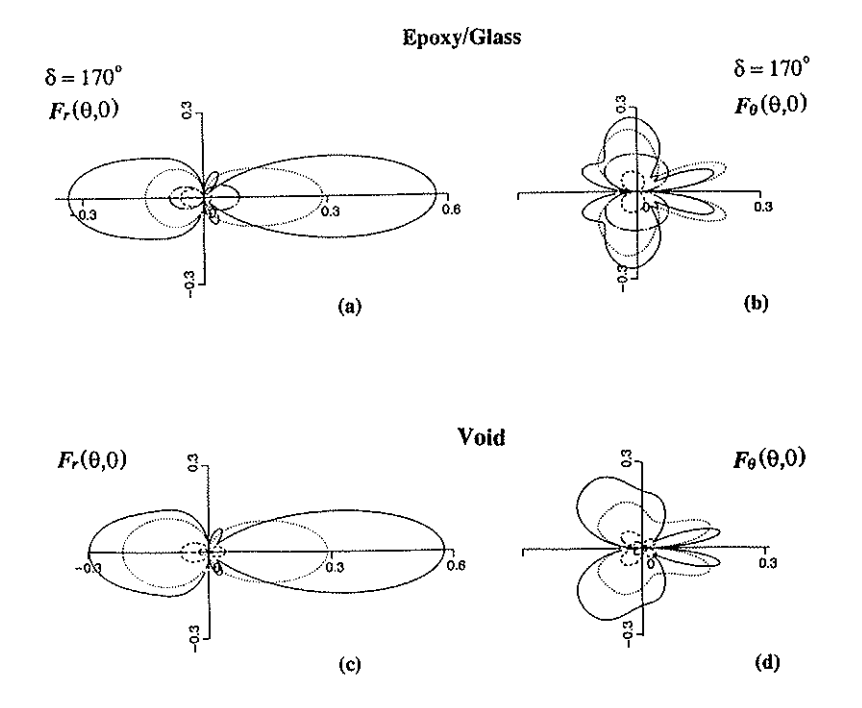


Fig. 6. The radiation patterns at the low frequency resonance, $k_{\perp}^{m}a = 0.22$ (chaindotted), and slightly off resonance $k_{\perp}^{m}a = 0.4$ (dash), 2 (dotted) and 4 (solid). The longitudinal and shear patterns for glass/epoxy are displayed in (a) and (b), respectively, those for a void are plotted in (c) and (d) for comparison.

the void are very similar to each other at the high frequencies $k_L^m a = 2$, 4, but quite different at the low resonance frequency $k_L^m a = 0.22$ and its nearby frequency 0.4. In Figs. 6(a) and (b) for $\delta = 170^\circ$, both the longitudinal and shear radiation patterns are almost symmetric in forward and backward scattering at the rattling resonance $k_L^m a = 0.22$, and they are much stronger than those at its nearby frequency 0.4; while in Figs. 6(c) and (d) for the void, the observations are just the opposite. These phenomena are consistent with those displayed in Fig. 5(b).

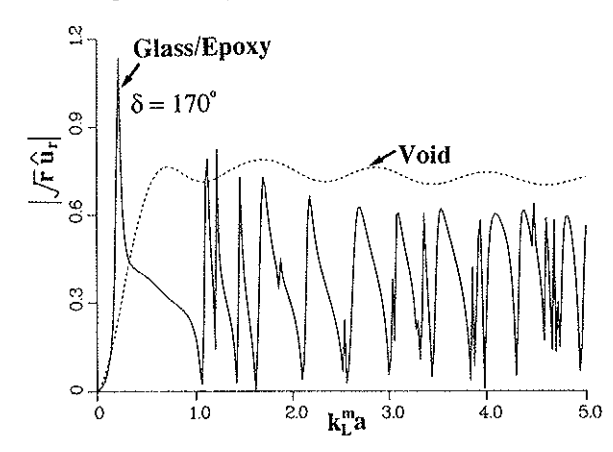


Fig. 7. The spectra of the far-field displacement in the radial direction for glass/epoxy at $\theta_0 = 0^\circ$, $\delta = 170^\circ$ (solid) and void (dash).

The harmonic solution to the displacement in the radial direction u_r in the far-field is plotted in Fig. 7 for $\delta = 170^{\circ}$ at $\theta = \pi$. It exhibits characteristics similar to those of the DSIF in Fig. 3. The transient response of the back-scattered displacement in the radial direction are illustrated in Figs. 8(a) and (b) for an incident longitudinal pulse of displacement assumed to be in the form of the Blackman window function (see the inset in Fig. 8(a)), defined by

$$u^{\text{in}}(t) = \begin{cases} \sum_{n=0}^{3} b_n \cos(2\pi nt/T), & \text{if } 0 \leq t \leq T, \\ 0, & \text{otherwise,} \end{cases}$$
 (76)

where $b_0 = 0.35869$, $b_1 = -0.48829$, $b_2 = 0.14128$, $b_3 = -0.01168$. In Fig. 8(a), the width of the pulse is chosen as $T = 20.4a/c_L^f$, the same period of the lowest resonance for $\delta = 170^\circ$, so that a strong resonance can be excited for that particular crack length. Figure 8(a) shows that the durations of the response for $\delta = 60^\circ$ and $\delta = 110^\circ$ are approximately equal to that of the incident pulse T, while for $\delta = 170^\circ$ the disturbance lasts much longer. It is evident from Fig. 8(b) that the frequency of the oscillation at $\delta = 170^\circ$ is independent of the incident pulse width and identical to its rattling resonance frequency. The mechanism is that when $0 \le t \le T$, the fiber experiences a forced vibration, then as the pulse passes by, the fiber oscillates freely at

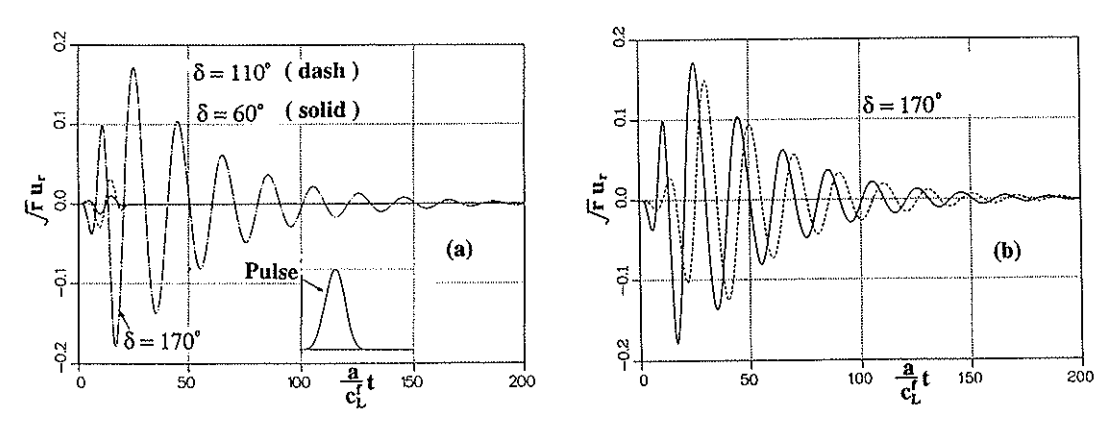


Fig. 8. The transient response of the far-field displacement in the radial direction for incidence of the Blackman window pulse at $\theta_0 = 0^\circ$: (a) the pulse duration $T = 20.4a/c_L^f$, (b) $T = 20.4a/c_L^f$ (solid), and $T = 30a/c_L^f$ (dash).

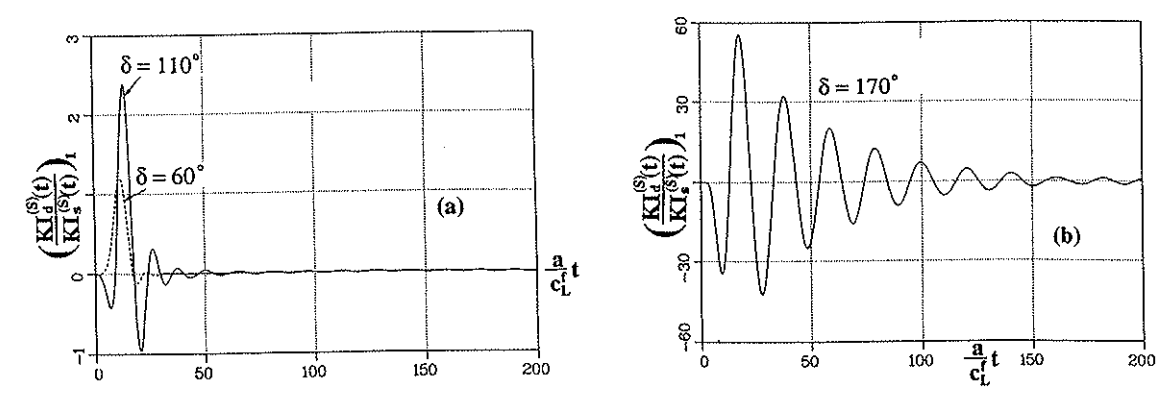


Fig. 9. The transient response of the ratio of the first dynamic SIF to the first static SIF for incidence of the Blackman window pulse at $\theta_0 = 0^\circ$ with pulse width $T = 20.4a/c_L^f$.

its resonance frequency with damping caused only by the radiation of energy into the matrix. In principle, once the rattling resonance frequency is determined, the crack length can be found directly from the numerical results for the time harmonic solution.

The dynamic effects on the stresses near the crack tips are illustrated in Figs. 9(a), (b) and Fig. 10, where the transient responses of the ratios of the first DSIF to the first static SIF and the second DSIF to the second static SIF are presented for the same incident pulse as in Fig. 8(a). It is noted that the dynamic SIF always overshoots the static SIF, particularly when the resonance of the fiber is excited, and the relative increase can be several orders of magnitude higher than the static value. Therefore, a relatively small amplitude incident pulse could excite a resonance and result in the propagation of the debond.

In conclusion, the present analysis and particularly the discussions on the rattling resonance indicate that the resonance may be an appreciable effect even at very low frequencies where Rayleigh scattering would normally be expected. The appearance of the resonance in the scattered fields suggests that it could be used in ultrasonic nondestructive evaluation to characterize large debonds in fiber reinforced composites.

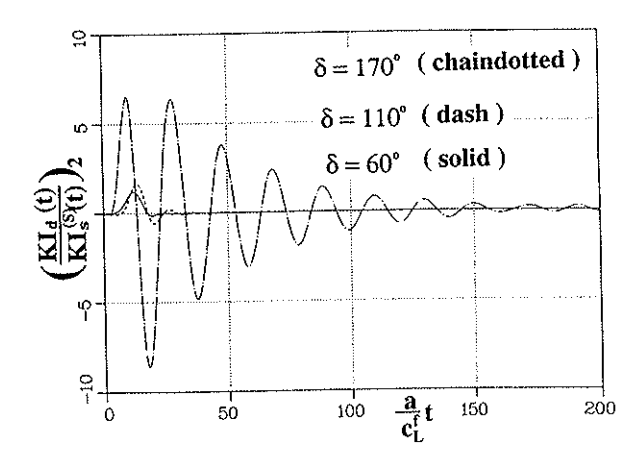


Fig. 10. The transient response of the ratio of the second dynamic SIF to the second static SIF for incidence of the Blackman window pulse of duration $T = 20.4a/c_L^2$, $\theta_0 = 0^\circ$.

Acknowledgment

We are grateful to the reviewers for helpful comments.

Appendix

The parameters $f(\theta)$ and $g(\theta)$ of (66) for $\xi = 1$ follow from Toya [12] as

$$f(\theta) = \frac{1}{2}(N_{\infty} + T_{\infty} - G)(\cos \theta - \cos \delta) + \frac{1}{2}H\sin \theta + \frac{2 - \beta}{2}(T_{\infty} - N_{\infty})[\cos(2\theta_{0} - \theta)\cos \delta - \cos 2(\theta_{0} - \theta)],$$

$$(77)$$

$$g(\theta) = \frac{1}{2}(N_{\infty} + T_{\infty} - G) \sin \theta - \frac{1}{2}H(\cos \theta - \cos \delta)$$

$$+\frac{2-\beta}{2}\left(T_{\infty}-N_{\infty}\right)\left[\sin(2\theta_{0}-\theta)\cos\delta-\sin2(\theta_{0}-\theta)\right],\tag{78}$$

where

$$\beta = \frac{4\mu_m (1 - \nu_f)}{\mu_m + (3 - 4\nu_m)\mu_f},\tag{79}$$

$$G = \left[(N_{\infty} + T_{\infty})(1 - \cos \delta) + \frac{2 - \beta}{2} (T_{\infty} - N_{\infty}) \sin^2 \delta \cos 2\theta_0 \right] \frac{\beta}{4 - \beta - \beta \cos \delta}, \tag{80}$$

$$H = (2 - \beta)(T_{\infty} - N_{\infty}) \sin^2\left(\frac{\delta}{2}\right) \sin 2\theta_0.$$
 (81)

References

- [1] E.A. Kraut, "Review of theories of scattering of elastic waves by cracks", *IEEE Trans. Sonics Ultrasonics 23*(3), 162-167 (May 1976)
- [2] F. Neerhoff, "Diffraction of love waves by a stress-free crack of finite width in the plane interface of a layered composite", Appl. Sci. Res. 35 (1979).
- [3] A. Boström, "Elastic wave scattering from an interface crack: antiplane strain", J. Appl. Mech. Trans. ASME 54, 503-508 (Sept. 1987).
- [4] O. Coussy, "Mécanique des solides élastiques", C. R. Acad Sci. Paris 295 (1982).
- [5] O. Coussy, "The influence of interface cracks on wave motion in fiber reinforced elastic solids", J. Mécanique Théorique et Appliquée 5 (1986).
- [6] Y. Yang and A.N. Norris, "Shear wave scattering from a debonded fibre", J. Mech. Phys. Solids 39(2), 273-294 (1991).
- [7] S. Krenk and H. Schmidt, "Elastic wave scattering by a circular crack", Phil. Trans. R. Soc. London, A 308 (1982).
- [8] A. Norris and Y. Yang, "Dynamic stress on a partially bonded fiber", J. Appl. Mech. Trans. ASME 58, 404-409 (June 1991).
- [9] A. Burrows, "Waves incident on a circular harbour", Proc. R. Soc. London, A 401, 349-371 (1985).
- [10] M. Kitahara, K. Nakagawa and J.D. Achenbach, "Backscatter from a spherical inclusion with complaint interphase characteristics", in: Proceedings of the 15th Annual Review of Progress in Quantitative Nondestructive Evaluation, pp. 47-54 (1988).
- [11] A. Boström and P. Olsson, "Scattering of elastic waves by non-planar cracks", Wave Motion 9, 61-76 (1987).
- [12] M. Toya, "A crack along the interface of a circular inclusion embedded in an infinite solid", J. Mech. Phys. Solids 22, 325-348 (1974).